Searching for patchy reionization from cosmic microwave background with hybrid quadratic estimators

Chang Feng and Gilbert Holder

Searching for patchy reionization from the cosmic microwave background with hybrid quadratic estimators

Chang Feng[1, *] and Gilbert Holder[1, 2, 3]

[1]*Department of Physics, University of Illinois at Urbana-Champaign,*
1110 West Green Street, Urbana, Illinois, 61801, USA
[2]*Department of Astronomy, University of Illinois at Urbana-Champaign,*
1002 West Green Street, Urbana, Illinois, 61801, USA
[3]*Canadian Institute for Advanced Research, Toronto, Ontario M5G 1M1, Canada*

We propose a hybrid quadratic estimator to measure cross correlations between gravitational lensing of the cosmic microwave background (CMB) and differential screening effects arising from fluctuations in the electron column density, such as those which could arise from patchy reionization. The hybrid quadratic estimators are validated by simulated data sets with both Planck and CMB-Stage 4 (CMB-S4) instrumental properties and found to be able to recover the cross-power spectra with almost no biases. We apply this technique to Planck 2015 temperature data and obtain cross-power spectra between gravitational lensing and differential screening effects. Planck data alone cannot detect the patchy-reionization-induced cross-power spectrum but future experiments like CMB-S4 will be able to robustly measure the expected signal and deliver new insights on reionization.

I. INTRODUCTION

Recombination of hydrogen atoms 379,000 years after the Big Bang left the early Universe with neutral hydrogen gas that was almost uniform but had small density fluctuations [1]. These fluctuations seeded the population of the first stars that emitted ultraviolet (UV) radiation, by which electrons were stripped from neutral hydrogen atoms and scattered with cosmic microwave background (CMB) photons. Large inhomogeneities in the ionization fraction of the gas were created during the so-called epoch of reionization (EoR), leading to substantial variations in the CMB scattering optical depth. At later times there are additional modulations in the scattering optical depth that arise from fluctuations in the baryon density. These variations in the scattering optical depth cause secondary fluctuations in the CMB.

The secondary CMB anisotropies generated at the EoR are extremely weak but can create excess power in CMB temperature and polarization power spectra [2]. However, it is very difficult to detect the small amount of excess power from these secondary anisotropies in the presence of the substantial fluctuation power coming from the (Gaussian) primary fluctuations and instrument noise. To get sufficient sensitivities, higher order estimators for patchy reionization have been developed with three-point [3] and four-point [4–7] correlation functions. However, they either rely on a high-redshift large scale structure tracer which is hard to obtain or contain significant higher order biases that introduce extra uncertainties for the measurements. Although the auto-power spectrum of patchy reionization can be recovered after subtracting model-dependent biases, a Gaussian noise that is almost six orders of magnitude higher than the signal makes it hard to detect.

Building on previous work [3] which investigated the utility of cross-correlating a relatively noisy optical depth reconstruction with higher signal-to-noise tracers of large scale structure, we consider the CMB gravitational lensing as a high-redshift tracer and construct a cross correlation between gravitational lensing (ϕ) and differential screening (τ) effects. This is essentially a four-point correlation function, using two-point estimators for ϕ and τ, respectively. In this paper, we study theoretical predictions of this cross correlation, and construct a hybrid quadratic estimator to extract such a signal from CMB data.

This paper is structured as follows: in Sec. II, we describe details of constructing the "hybrid quadratic estimator" as well as various debiasing steps; in Sec. III, we validate the hybrid quadratic estimator with simulations at noise levels appropriate for Planck and a CMB-S4-like experiment; we then apply this estimator to Planck 2015 temperature data in Sec. IV and conclude in Sec. V.

II. HYBRID QUADRATIC ESTIMATORS

The CMB with both gravitational lensing (ϕ) and differential screening (τ) effects can be projected onto a unit sphere as

$$X(\mathbf{n}) = \tilde{X}(\mathbf{n} + \nabla\phi(\mathbf{n}))e^{-\tau(\mathbf{n})}, \qquad (1)$$

where $\mathbf{n}$ is a direction in the sky and $\tilde{X}$ is the unlensed CMB. The symbol X refers to the lensed CMB (or the measured CMB) and it can be CMB temperature T or polarization $Q \pm iU$. For CMB measurements, it is customary to express polarization measurements in terms of electric-like (E) and curl-like (B)

modes. These are related to the Stokes parameters via $Q \pm iU = -\sum_{\ell m}(E_{\ell m} \pm iB_{\ell m})_{\pm 2}Y_{\ell m}$ where $_sY_{\ell m}$ are spin-s spherical harmonics.

Noisy reconstructions of ϕ and τ [4, 8] are proportional to off-diagonal elements of the covariance matrix for two CMB modes $X_{\ell m}$ and $Z_{\ell' m'}$. In essence, a general form for any noisy reconstruction can be expressed as

$$\Psi_{LM}^{(c)}(X_{\ell m}, Z_{\ell' m'}) = A_L^{(c)} \sum_{\ell m \ell' m'} (-1)^M \begin{pmatrix} \ell & \ell' & L \\ m & m' & -M \end{pmatrix}$$
$$\times g_{\ell \ell'}^{(c)}(L) X_{\ell m} Z_{\ell' m'}, \tag{2}$$

where the modes $X_{\ell m}$ and $Z_{\ell' m'}$ can be $T_{\ell m}$ for temperature, and $E_{\ell m}/B_{\ell m}$ modes for polarization. The big bracket (...) is the 3-j Wigner symbol. Normalization functions A_L and weighting functions $g_{\ell \ell'}(L)$ are given in [4, 8] for ϕ and τ, respectively. The superscript "(c)" = $\{\phi, \tau\}$ and quadratic estimators for lensing and anisotropic optical depth are $\Psi^{(\phi)} = \hat{\phi}$ and $\Psi^{(\tau)} = \hat{\tau}$, respectively. A hybrid quadratic estimator is defined as the cross power spectrum between these two reconstructed fields, $\hat{C}_\ell^{\phi\tau}\delta_{\ell\ell'}\delta_{mm'} = \langle\Psi_{\ell m}^{(\phi)}\Psi_{\ell' m'}^{(\tau,*)}\rangle$. The weighting function $g_{\ell\ell'}^{(c)}(L)$ has a separable form and the hybrid quadratic estimators can be expressed as products of filtered maps, thereby computation cost is significantly reduced [9].

We make a set of simulations $\{\hat{\phi}^{(un)}, \hat{\phi}^{(\phi)}, \hat{\phi}^{(\tau)}, \hat{\phi}^{(f)}, \hat{\phi}^{(G)}\}$ for lensing potential and an analogous set of simulations for τ. Here the superscripts "(un)", "(ϕ)", "(τ)", "(f)" and "(G)", refer to unlensed maps, lensed maps, maps only perturbed by τ, maps with both ϕ and τ perturbations, and Gaussian simulations from lensed CMB power spectra. A four-point correlation function is thus constructed from four CMB maps X, Z, W and V:

$$\hat{C}_\ell^{\phi\tau} = \langle[\hat{\phi}(X^{(s)}, Z^{(s)}) - \hat{\phi}(X^{(\tau)}, Z^{(\tau)})]$$
$$\times [\hat{\tau}(W^{(s)}, V^{(s)}) - \hat{\tau}(W^{(\phi)}, V^{(\phi)})]\rangle, \tag{3}$$

where the superscript "(s)" refers to data or simulations, and applies to both lensing potential ϕ and CMB realizations (X, Z, W, V). Maps $\hat{\phi}(X^{(\tau)}, Z^{(\tau)})$ are lensing reconstructions from CMB realizations $X^{(\tau)}$ and $Z^{(\tau)}$ which are unlensed CMB but perturbed by τ signal only. Maps $\hat{\tau}(W^{(\phi)}, V^{(\phi)})$ are reconstructions of the optical depth from lensed CMB realizations $W^{(\phi)}$ and $V^{(\phi)}$. The $\hat{\phi}^{(\tau)}$ could be affected by a different EoR model, but it is a very negligible correction to $\hat{\phi}^{(s)}$ so the bias due to a EoR-model mismatch is negligible. We will use numerical simulations to validate that unbiased reconstructions of the cross-power spectrum are always obtained with very different EoR models. Mean field maps derived from simulations are subtracted from measured ϕ and τ reconstructions. An estimator-based bias [Eqs. (A5) or (A9)] is subtracted from a raw signal-plus-noise trispectrum in addition to the Gaussian and higher order biases (N_1). To account for any potential covariance mismatch between data and simulations, a realization dependent bias
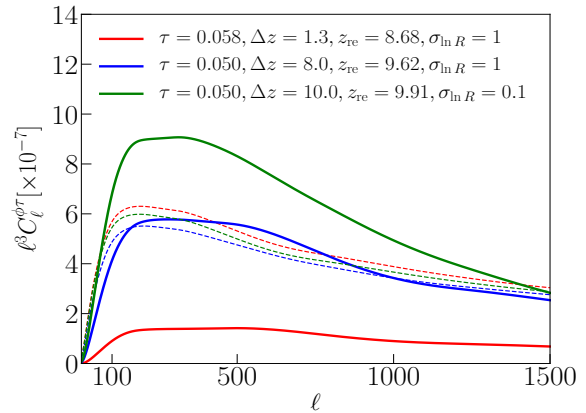

FIG. 1. Theoretical cross-correlations $\langle\phi\tau\rangle$ between CMB gravitational lensing and differential screening effects. Contributions by patchy reionization (solid) and large scale structure (dashed) are shown with three EoR models. It is seen that the cross-power spectrum $\langle\phi\tau\rangle$ due to patchy reionization has a consistent shape but could have different amplitudes. The theoretical predictions in the green curves are calculated with assumptions that bubble size ($\bar{R}$) and bubble bias (b_{bubble}) are free parameters as done in [4]. The parameter z_{re} in the legend is a characteristic redshift for an ionization history and is determined by the optical depth today and the duration of EoR.

is subtracted from the measured raw trispectra instead of the simulated Gaussian bias [Eq. (A2)] [10, 11]. We will verify in the next section that the higher order biases are negligible for the cross-power spectrum $\langle\phi\tau\rangle$ with different amplitudes predicted by a broad range of EoR models, but may not be negligible for the auto-power spectrum $\langle\tau\tau\rangle$ if its amplitude is too low.

III. NUMERICAL VALIDATIONS

We simulate CMB temperature and polarization for a next generation experiment like CMB-S4 with noise levels at $\Delta_T = 1\mu$K-arcmin and $\Delta_P = \sqrt{2}\mu$K-arcmin [12]. We assume a Gaussian beam with $\theta = 1'$ full width at half maximum and a full-sky coverage. The unlensed CMB power spectra are calculated by CAMB [1]. The lensed CMB simulations are made by *Taylens* [13] at HEALPix [14] resolution $N_{\text{side}} = 2048$. Patchy-reionization-related theory power spectra $C_\ell^{\tau\tau}$ and $C_\ell^{\phi\tau}$ are calculated using the halo model formalism [15, 16], in which the CAMB's tanh reionization model is used [17] and the size of ionizing bubbles is assumed to satisfy a logarithmic distribution [18]. The bubble size and bubble bias are self-consistently solved for a given reionization history. The fiducial parameters for the EoR are
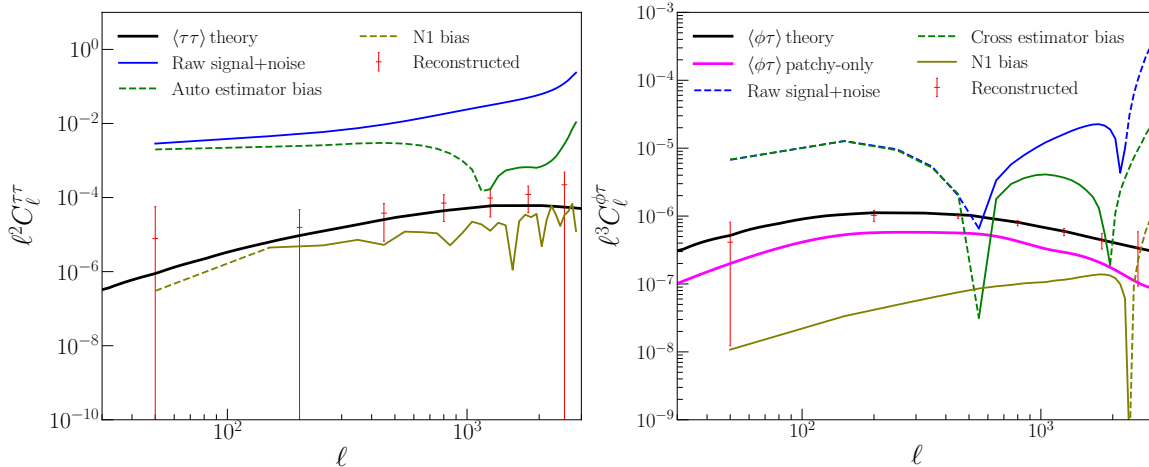
---

[1] https://camb.info

FIG. 2. Comparison of the auto-power spectrum estimator $\langle\tau\tau\rangle$ (left) and the cross-power spectrum estimator $\langle\phi\tau\rangle$, i.e., the hybrid quadratic estimator, with a CMB-S4-like data set. Here we only show detailed components for $\langle\tau(EB)\tau(EB)\rangle$ (left) and $\langle\phi(EB)\tau(EB)\rangle$ (right). The dashed portion is negative. Signal-to-noise ratios for the auto- and the cross-power spectra with the fiducial EoR model are $\sim 2\sigma$ and $\sim 22\sigma$, respectively. The CMB modes within $200 < \ell < 3000$ are used for the reconstructions and the error bars are calculated from 200 signal-plus-noise simulations.
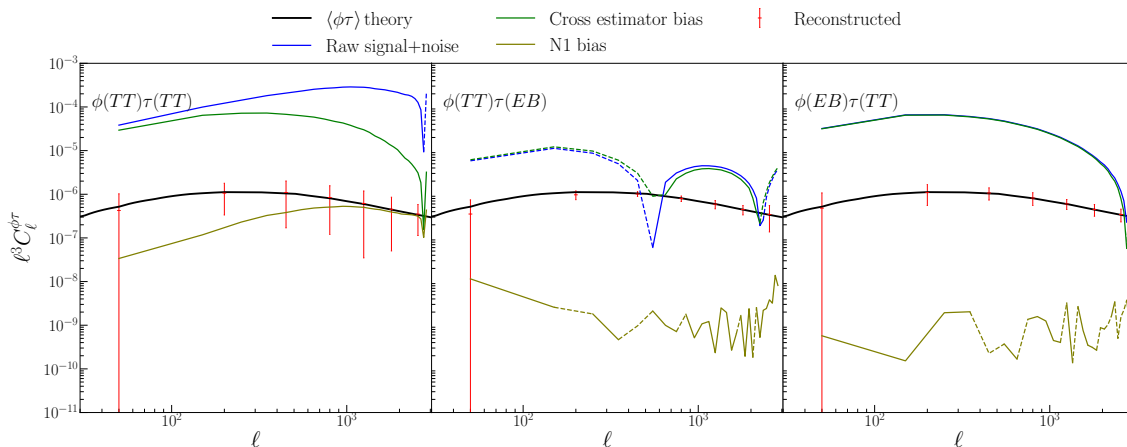

FIG. 3. Validations of the hybrid quadratic estimators with a CMB-S4-like data set. Simulations are made at HEALPIX resolution $N_{\mathrm{side}} = 2048$. The signal-to-noise ratios are 4σ for $\langle\phi(TT)\tau(TT)\rangle$, 14σ for $\langle\phi(TT)\tau(EB)\rangle$, 9σ for $\langle\phi(EB)\tau(TT)\rangle$ and 22σ for $\langle\phi(EB)\tau(EB)\rangle$ [Fig. 2 (right)], respectively. The CMB modes within $200 < \ell < 3000$ are used for the reconstructions. The dashed portion is negative.

$\{\tau = 0.05, \Delta z = 8, \sigma_{\ln R} = 1\}$, where τ is the optical depth today [19], Δz is duration of the EoR and $\sigma_{\ln R}$ is the variance of the ionizing bubbles. A representative plot for the cross-power spectrum $C_\ell^{\phi\tau}$ is shown in Fig. 1, where a calculation made by a toy model, assuming the bubble size $\bar{R}$ and bubble bias b_{bubble} are free parameters, is also shown in green for comparison [4]. From definition, electron density is a function of both free electron fraction and baryon density so fluctuations of the optical depth can be decomposed into two main pieces, ionizing field and matter density. The cross-power spectrum $C_\ell = C_\ell^{\mathrm{patchy}} + C_\ell^{\mathrm{LSS}}$, where C_ℓ^{patchy} is the theoret-

ical cross-power spectrum created by patchy reionization (blue solid line in Fig. 1), and C_ℓ^{LSS} is the cross-power spectrum due to the low-z large scale structure (LSS, blue dashed line in Fig. 1). From a family of cross-power spectra, it is seen that the large-scale-structure (LSS) generated piece has a weak dependence on the EoR models, but the one generated by patchy reionization has a very uncertain amplitude.

We made simulations for ϕ_{input} and τ_{input} by performing the Cholesky decomposition of the theoretical covariance between them. These simulations are used as input for generation of mock CMB data. For a CMB-S4-like experiment, we make white noise simulations and con-
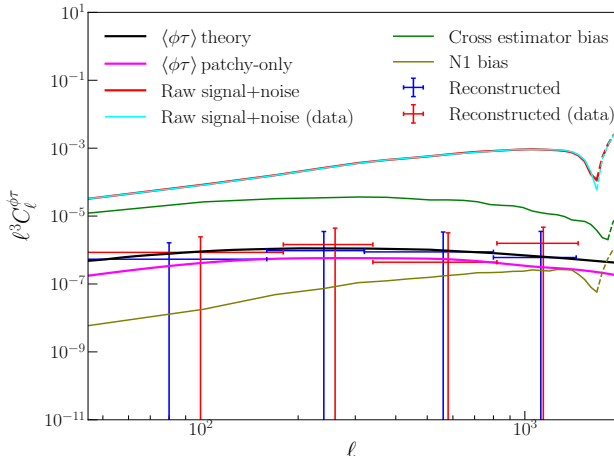
FIG. 4. Cross-power spectrum $\langle\phi\tau\rangle$ for Planck simulations and data. Planck full focal plane simulations FFP8.1 are used for the noise component. The dashed portion is negative.

volve mock CMB maps with the beam profile. We apply the estimators Ψ (Eq. (2)) to the mock CMB data and create reconstructed $\hat{\phi}$ and $\hat{\tau}$ maps. We validate that the cross-power spectra $\langle\hat{\phi}\phi_{\text{input}}\rangle$ and $\langle\hat{\tau}\tau_{\text{input}}\rangle$ are consistent with input power spectra $C_\ell^{\phi\phi}$ and $C_\ell^{\tau\tau}$.

After subtracting the biases calculated using simulations, the cross-power spectrum $\langle\phi\tau\rangle$ can be recovered as Fig. 2 shows. A residual bias, that is smaller than the statistical uncertainty, is seen from the auto-power spectrum $\langle\tau\tau\rangle$. Since the residual bias of the auto-power spectrum is EoR-model dependent, it would become negligible if the amplitude of the input model $\langle\tau\tau\rangle$ is lower than our nominal model. The sensitivity of the reconstructed auto-power spectrum is much lower than the cross-power spectrum $\langle\phi\tau\rangle$ that is derived from the same reionization model as seen from the error bars averaged from 200 signal-plus-noise simulations. Also, the auto-power spectrum $\langle\tau\tau\rangle$ may strongly depend on the higher order bias (N_1) that must be determined from the desired patchy reionization signal, and model uncertainty will complicate interpretations of data measurements. On the other hand, the numerical simulations show that the reconstructed cross-power spectra $\langle\phi\tau\rangle$ have negligible higher order biases and a precise knowledge of the reionization model is not required. We validated this by repeating the same calculation with a minimum EoR model [red curves in Fig. (1)] and we found that the auto- and cross-power spectra are both correctly recovered, and the higher order biases are negligible for the cross but not for the auto. This can be understood intuitively: the cross-power spectrum $\langle\phi\tau\rangle$ only relies on $\mathcal{O}(\tau)$ not $\mathcal{O}(\tau^2)$, so it is less dependent of the poorly known reionization model.

In Fig. 3, we show various components generated by the $\langle\phi\tau\rangle$ hybrid quadratic estimators with CMB temperature and polarization simulations and validate that the

hybrid quadratic estimators can recover the cross-power spectrum $C_\ell^{\phi\tau}$ from different CMB combinations. The calculation shows that, for a CMB-S4-like experiment, most of the signal-to-noise comes from the polarization trispectrum $\langle EBEB\rangle$ and the total signal-to-noise ratio would reach a $\sim 30\sigma$ level if all the cross-power spectra are combined. This cross-spectrum is a four-point correlation function resembling the reconstructed lensing power spectrum, but applies different filters to the various mode pairs. It is still an internal measurement that only uses CMB data as an external large scale structure tracer is not required.

Signal-to-noise ratios (SNRs) for the cross-power spectra $\langle\phi\tau\rangle$ are roughly one order of magnitude higher than the auto-power spectra $\langle\tau\tau\rangle$. The higher SNRs of the hybrid quadratic estimator can be easily understood by introducing a reconstruction noise for the hybrid quadratic estimator, i.e., $N_0^{\phi\tau} \propto \sqrt{N_0^{\phi\phi}N_0^{\tau\tau}}$, from which the SNR ratio of hybrid quadratic estimator to $\langle\tau\tau\rangle$ can be approximated by the Knox formula as a scaling law $\sqrt{N_0^{\tau\tau}/N_0^{\phi\phi}}(C_\ell^{\phi\tau}/C_\ell^{\tau\tau})$ which is dominated by the noise ratio $\sqrt{N_0^{\tau\tau}/N_0^{\phi\phi}}$. Here $N_0^{\phi\phi}$ and $N_0^{\tau\tau}$ are reconstruction noises of the estimators Ψ in Eq. (2). The reconstruction noise comes from disconnected pieces of the four-point correlation functions and does not vanish even if the CMB simulations are unlensed. Theoretical calculations show that $N_0^{\phi\phi} \ll N_0^{\tau\tau}$ for next generation CMB data sets, so the ratio $\sqrt{N_0^{\tau\tau}/N_0^{\phi\phi}} \gg 1$, which means $\langle\phi\tau\rangle$ will be more sensitive than $\langle\tau\tau\rangle$.

IV. MEASUREMENTS FROM PLANCK 2015 TEMPERATURE DATA

To measure a cross-power spectrum $\langle\phi\tau\rangle$ from data with the hybrid quadratic estimator, we use the 2015 Planck SMICA temperature data [20]. It is foreground-cleaned and is less contaminated by foregrounds than single frequency maps. The beam profile of SMICA data can be well approximated as a $5'$ Gaussian beam. An analysis mask is applied to remove point sources and Galactic plane, resulting in a sky fraction $f_{\text{sky}} = 0.67$. The mask is apodized with $60'$ Gaussian beam to suppress mode-mixing induced by the sky cut. To reduce potential systematic effects and dust contamination, we filter out the data below $\ell_{\text{min}} = 200$. We also set $\ell_{\text{max}} = 2048$ to avoid potential high-ℓ foreground residuals. We use the Planck full focal plane (FFP) simulation, i.e., FFP8.1 SMICA noise simulations [21] [2], and have checked that the noise

———

[2] https://crd.lbl.gov/departments/computational-science/c3/c3-research/cosmic-microwave-background/cmb-data-at-nersc/
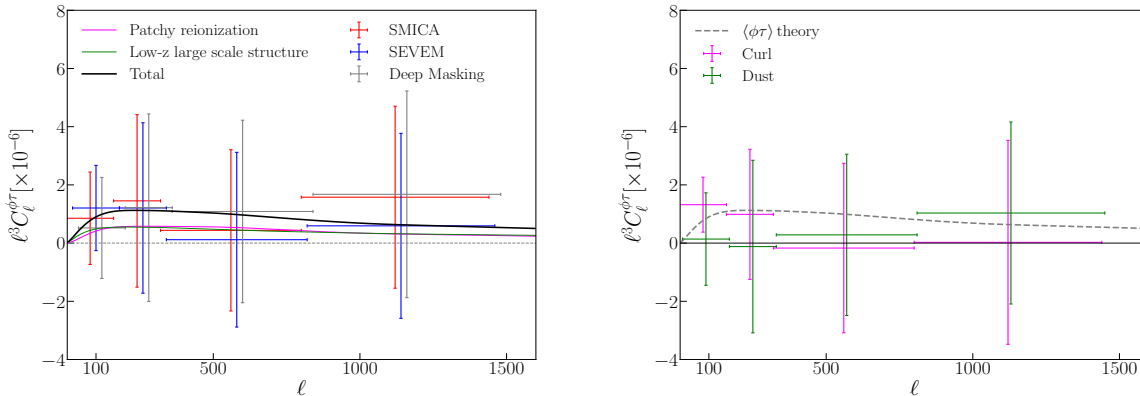
FIG. 5.   Left: measured cross-power spectrum $\langle\phi\tau\rangle$ from 2015 Planck component-separated temperature maps SMICA and SEVEM. Right: systematic tests for the Planck SMICA data.
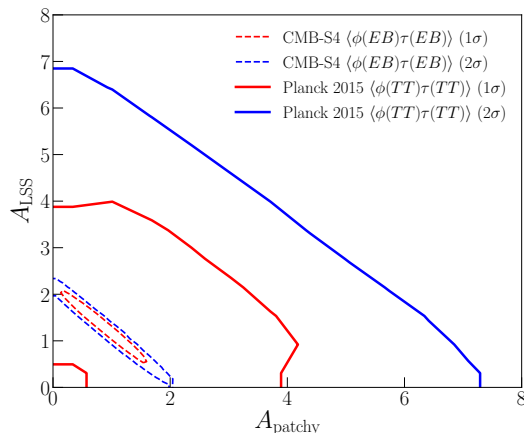

FIG. 6. Constraints on component amplitudes for the cross-power spectra $\langle\phi\tau\rangle$ generated by patchy reionization and large scale structure, respectively. Planck and CMB-S4-like constraints are shown in solid and dashed lines, respectively.

power spectra from SMICA component-separation simulations can precisely match the measured ones.

The reconstructions with the hybrid quadratic estimators are performed with a full suite of Planck simulations. We have repeated the same validation procedures, as for the CMB-S4-like experiment in the previous section, for the Planck 2015 data. We show different components of the cross-power spectrum $\langle\phi\tau\rangle$ for the Planck 2015 simulations in Fig. 4, where a bias-free reconstruction (blue band powers) of the cross-power spectrum $\langle\phi\tau\rangle$ is achieved after subtracting simulation-derived biases. We only use the Planck temperature data, as the polarization data are too noisy to be used for this analysis.

In Fig. 5 (left), we show the measured cross-power spectra $\langle\phi\tau\rangle$ from Planck temperature maps that are separated from raw data using component-separation meth-

ods SMICA and SEVEM [20]. In the right panel of Fig. 5, we show that the cross-power spectra due to foregrounds and systematic effects are consistent with zero. To constrain the EoR models, we compare the theoretical models to the measurement and calculate a χ^2 from

$$\chi^2 = \sum_{bb'}(\hat{C}_b - C_b^{\rm th})\mathbf{C}_{bb'}^{-1}(\hat{C}_{b'} - C_{b'}^{\rm th}). \qquad (4)$$

Here $\mathbf{C}$ is the covariance matrix between different band powers and $\hat{C}_b$ is the measured $\langle\phi\tau\rangle$ band power at band b. The theoretical band power is decomposed into two parts: $C_b^{\rm th} = \mathcal{A}_{\rm patchy}C_b^{\rm patchy} + \mathcal{A}_{\rm LSS}C_b^{\rm LSS}$, where $C_b^{\rm patchy}$ is the theoretical cross-power spectrum created by patchy reionization (blue solid line in Fig. 1), and $C_b^{\rm LSS}$ is the cross-power spectrum due to the low-z large scale structure (LSS, blue dashed line in Fig. 1). This simple parametrization is chosen to avoid degeneracy of the EoR parameters which are still difficult to be constrained from this measurement.

In Fig. 6, we show 1σ and 2σ bounds on the parameters $\mathcal{A}_{\rm patchy}$ and $\mathcal{A}_{\rm LSS}$ for Planck 2015 measurements from $\langle\phi(TT)\tau(TT)\rangle$ and CMB-S4 from $\langle\phi(EB)\tau(EB)\rangle$. The anti-correlation between the two amplitudes is shown in Fig. 6 if both amplitudes are varied. Given the fact that the LSS contribution $\mathcal{A}_{\rm LSS}$ does not vary too much as seen from the theoretical calculations in Fig. 1, we fix $\mathcal{A}_{\rm LSS}$ to be 1 and find that $\mathcal{A}_{\rm patchy} < 6$ at 95% confidence level. Compared to the fiducial model ($\mathcal{A}_{\rm patchy}=1$, $\mathcal{A}_{\rm LSS} = 1$), the SMICA measurement (red data points) has an overall amplitude $\mathcal{A} < 3$ at 95% confidence level, and the $\chi^2/\rm dof$ is found to be $0.22/4$. We replace the SMICA map by SEVEM and use its FFP8 noise simulations. The same analysis is performed and the measurement (in blue) is consistent with the one from SMICA data. Moreover, we test a deeper masking scheme for the SMICA data and find that a more expansive sky cut with $f_{\rm sky} \sim 0.57$ results in a negligible change to the cross-power spectrum [Fig. 5 (left)].

From the Planck temperature data, the cross-power spectrum $\langle\phi\tau\rangle$ is not detected (at $\sim 1\sigma$ statistical significance level), but will be detected by the CMB-S4-like experiment, and the parameter space on the $\mathcal{A}_{\text{patchy}}-\mathcal{A}_{\text{LSS}}$ plane will be significantly reduced as seen from Fig. 6, where only simulated band powers from $\langle\phi(EB)\tau(EB)\rangle$ are taken into account.

Foregrounds and systematic effects could generate spurious $\langle\phi\tau\rangle$ cross-power spectra so we perform different tests to estimate these biases. We construct a curl null estimator [22] for the lensing potential and use it to measure the cross-power spectrum $\langle\phi^{\text{curl}}\tau\rangle$ with an expected signal of zero. In Fig. 5 (right), it is found to be consistent with zero and the PTE is 79%. Given the fact that the SMICA data is foreground-cleaned and only the temperature modes within $200 < \ell < 2048$ are used, contaminating power of dust and foregrounds on the cross-power spectrum $\langle\phi\tau\rangle$ should be negligible. To verify this, we investigate the maximum impact with no dust isolation and propagate a Planck thermal dust map "COM_CompMap_dust-commrul_2048_R1.00.fits" through the same analysis pipeline. The dust-induced trispectrum $\langle\phi\tau\rangle$ shown in green in Fig. 5 (right) is consistent with zero.

For the next generation experiments such CMB-S4, the hybrid quadratic estimators will be applied to data at much broader angular ranges where other contaminants like thermal/kinetic Sunyaev-Zel'dovich effects (tSZ/kSZ) will come into play. These contaminants are correlated with the optical depth and lensing potential so biases might be introduced to the hybrid quadratic estimators. Moreover, the SNRs can be further boosted by incorporating an iterative maximum likelihood technique in the future CMB data sets. Detailed discussions for all of these issues are beyond the scope of this paper and we defer it to a full study in future work.

V. CONCLUSIONS

In this paper, we propose a hybrid quadratic estimator formalism for the study of fluctuations in the anisotropic optical depth, such as would be induced by patchy reionization. We make mock data sets for Planck and CMB-S4-like experiments and numerically validate that the cross-power spectrum $\langle\phi\tau\rangle$ can be correctly recovered from the CMB data alone. Moreover, we measure a $\langle\phi\tau\rangle$ cross-power spectrum from Planck 2015 temperature data and obtain a new upper bound for patchy reionization. Various systematic and foreground tests are performed and their effects are found to be negligible. For the next-generation CMB experiments, both temperature and polarization data can be used to measure the cross-power spectra $\langle\phi\tau\rangle$ with much higher signal-to-noise ratios, and the signal of patchy reionization in future experiments will be detected from CMB alone. These measurements made at microwave wavelengths and linear angular scales will complement current studies of reionization from 21 cm lines and kSZ, from which good priors on τ could also be obtained. However, to make a robust detection, we should make efforts to suppress impacts of polarized foregrounds, such as tSZ, and control instrumental systematic effects, such as differential beam and polarization angle etc. A detection of the cross-power spectrum $\langle\phi\tau\rangle$ will extend CMB science to a new regime when the first stars and galaxies formed.

VI. ACKNOWLEDGMENTS

[1] A. Loeb and R. Barkana, Ann.Rev.Astron.Astrophys. **39**, 19 (2001), astro-ph/0010467.

[2] C. Dvorkin, W. Hu, and K. M. Smith, Phys. Rev. D **79**, 107302 (2009), arXiv:0902.4413 [astro-ph.CO].

[3] C. Feng and G. Holder, ArXiv e-prints (2018), arXiv:1801.05396.

[4] C. Dvorkin and K. M. Smith, Phys. Rev. D **79**, 043003 (2009), arXiv:0812.1566.

[5] M. Su, A. P. S. Yadav, M. McQuinn, J. Yoo, and M. Zaldarriaga, ArXiv e-prints (2011), arXiv:1106.4313 [astro-ph.CO].

[6] V. Gluscevic, M. Kamionkowski, and D. Hanson, Phys. Rev. D **87**, 047303 (2013), arXiv:1210.5507 [astro-ph.CO].

[7] T. Namikawa, Phys. Rev. D **97**, 063505 (2018), arXiv:1711.00058.

[8] T. Okamoto and W. Hu, Phys. Rev. D **67**, 083002 (2003), astro-ph/0301031.

[9] Planck Collaboration, P. A. R. Ade, N. Aghanim, M. Arnaud, M. Ashdown, J. Aumont, C. Baccigalupi, A. J. Banday, R. B. Barreiro, J. G. Bartlett, and et al., Astron. Astrophys. **594**, A15 (2016), arXiv:1502.01591.

[10] Planck Collaboration, P. A. R. Ade, N. Aghanim, C. Armitage-Caplan, M. Arnaud, M. Ashdown, F. Atrio-Barandela, J. Aumont, C. Baccigalupi, A. J. Banday, and et al., Astron. Astrophys. **571**, A17 (2014),

arXiv:1303.5077.

[11] K. T. Story, D. Hanson, P. A. R. Ade, K. A. Aird, J. E. Austermann, J. A. Beall, A. N. Bender, B. A. Benson, L. E. Bleem, J. E. Carlstrom, C. L. Chang, H. C. Chiang, H.-M. Cho, R. Citron, T. M. Crawford, A. T. Crites, T. de Haan, M. A. Dobbs, W. Everett, J. Gallicchio, J. Gao, E. M. George, A. Gilbert, N. W. Halverson, N. Harrington, J. W. Henning, G. C. Hilton, G. P. Holder, W. L. Holzapfel, S. Hoover, Z. Hou, J. D. Hrubes, N. Huang, J. Hubmayr, K. D. Irwin, R. Keisler, L. Knox, A. T. Lee, E. M. Leitch, D. Li, C. Liang, D. Luong-Van, J. J. McMahon, J. Mehl, S. S. Meyer, L. Mocanu, T. E. Montroy, T. Natoli, J. P. Nibarger, V. Novosad, S. Padin, C. Pryke, C. L. Reichardt, J. E. Ruhl, B. R. Saliwanchik, J. T. Sayre, K. K. Schaffer, G. Smecher, A. A. Stark, C. Tucker, K. Vanderlinde, J. D. Vieira, G. Wang, N. Whitehorn, V. Yefremenko, and O. Zahn, Astrophys. J. **810**, 50 (2015), arXiv:1412.4760.

[12] K. N. Abazajian, P. Adshead, Z. Ahmed, S. W. Allen, D. Alonso, K. S. Arnold, C. Baccigalupi, J. G. Bartlett, N. Battaglia, B. A. Benson, C. A. Bischoff, J. Borrill, V. Buza, E. Calabrese, R. Caldwell, J. E. Carlstrom, C. L. Chang, T. M. Crawford, F.-Y. Cyr-Racine, F. De Bernardis, T. de Haan, S. di Serego Alighieri, J. Dunkley, C. Dvorkin, J. Errard, G. Fabbian, S. Feeney, S. Ferraro, J. P. Filippini, R. Flauger, G. M. Fuller, V. Gluscevic, D. Green, D. Grin, E. Grohs, J. W. Henning, J. C. Hill, R. Hlozek, G. Holder, W. Holzapfel, W. Hu, K. M. Huffenberger, R. Keskitalo, L. Knox, A. Kosowsky, J. Kovac, E. D. Kovetz, C.-L. Kuo, A. Kusaka, M. Le Jeune, A. T. Lee, M. Lilley, M. Loverde, M. S. Madhavacheril, A. Mantz, D. J. E. Marsh, J. McMahon, P. D. Meerburg, J. Meyers, A. D. Miller, J. B. Munoz, H. N. Nguyen, M. D. Niemack, M. Peloso, J. Peloton, L. Pogosian, C. Pryke, M. Raveri, C. L. Reichardt, G. Rocha, A. Rotti, E. Schaan, M. M. Schmittfull, D. Scott, N. Sehgal, S. Shandera, B. D. Sherwin, T. L. Smith, L. Sorbo, G. D. Starkman, K. T. Story, A. van Engelen, J. D. Vieira, S. Watson, N. Whitehorn, and W. L. Kimmy Wu, arXiv e-prints , arXiv:1610.02743 (2016), arXiv:1610.02743 [astro-ph.CO].

[13] S. K. Næss and T. Louis, J. Cosmol. Astropart. Phys. **9**, 001 (2013), arXiv:1307.0719.

[14] K. M. Górski, E. Hivon, A. J. Banday, B. D. Wandelt, F. K. Hansen, M. Reinecke, and M. Bartelmann, Astrophys. J. **622**, 759 (2005), astro-ph/0409513.

[15] A. Cooray and R. Sheth, Phys. Rep. **372**, 1 (2002), astro-ph/0206508.

[16] P. D. Meerburg, C. Dvorkin, and D. N. Spergel, Astrophys. J. **779**, 124 (2013), arXiv:1303.3887.

[17] A. Lewis, Phys. Rev. D **78**, 023002 (2008), arXiv:0804.3865.

[18] A. Lidz, O. Zahn, S. R. Furlanetto, M. McQuinn, L. Hernquist, and M. Zaldarriaga, Astrophys. J. **690**, 252 (2009), arXiv:0806.1055.

[19] Planck Collaboration, N. Aghanim, Y. Akrami, M. Ashdown, J. Aumont, C. Baccigalupi, M. Ballardini, A. J. Banday, R. B. Barreiro, N. Bartolo, S. Basak, R. Battye, K. Benabed, J. P. Bernard, M. Bersanelli, P. Bielewicz, J. J. Bock, J. R. Bond, J. Borrill, F. R. Bouchet, F. Boulanger, M. Bucher, C. Burigana, R. C. Butler, E. Calabrese, J. F. Cardoso, J. Carron, A. Challinor, H. C. Chiang, J. Chluba, L. P. L. Colombo, C. Combet, D. Contreras, B. P. Crill, F. Cuttaia, P. de Bernardis, G. de Zotti, J. Delabrouille, J. M. Delouis, E. Di Valentino, J. M. Diego, O. Doré, M. Douspis, A. Ducout, X. Dupac, S. Dusini, G. Efstathiou, F. Elsner, T. A. Enßlin, H. K. Eriksen, Y. Fantaye, M. Farhang, J. Fergusson, R. Fernandez-Cobos, F. Finelli, F. Forastieri, M. Frailis, E. Franceschi, A. Frolov, S. Galeotta, S. Galli, K. Ganga, R. T. Génova-Santos, M. Gerbino, T. Ghosh, J. González-Nuevo, K. M. Górski, S. Gratton, A. Gruppuso, J. E. Gudmundsson, J. Hamann, W. Hand ley, D. Herranz, E. Hivon, Z. Huang, A. H. Jaffe, W. C. Jones, A. Karakci, E. Keihänen, R. Keskitalo, K. Kiiveri, J. Kim, T. S. Kisner, L. Knox, N. Krachmalnicoff, M. Kunz, H. Kurki-Suonio, G. Lagache, J. M. Lamarre, A. Lasenby, M. Lattanzi, C. R. Lawrence, M. Le Jeune, P. Lemos, J. Lesgourgues, F. Levrier, A. Lewis, M. Liguori, P. B. Lilje, M. Lilley, V. Lindholm, M. López-Caniego, P. M. Lubin, Y. Z. Ma, J. F. Macías-Pérez, G. Maggio, D. Maino, N. Mandolesi, A. Mangilli, A. Marcos-Caballero, M. Maris, P. G. Martin, M. Martinelli, E. Martínez-González, S. Matarrese, N. Mauri, J. D. McEwen, P. R. Meinhold, A. Melchiorri, A. Mennella, M. Migliaccio, M. Millea, S. Mitra, M. A. Miville-Deschênes, D. Molinari, L. Montier, G. Morgante, A. Moss, P. Natoli, H. U. Nørgaard-Nielsen, L. Pagano, D. Paoletti, B. Partridge, G. Patanchon, H. V. Peiris, F. Perrotta, V. Pettorino, F. Piacentini, L. Polastri, G. Polenta, J. L. Puget, J. P. Rachen, M. Reinecke, M. Remazeilles, A. Renzi, G. Rocha, C. Rosset, G. Roudier, J. A. Rubiño-Martín, B. Ruiz-Granados, L. Salvati, M. Sandri, M. Savelainen, D. Scott, E. P. S. Shellard, C. Sirignano, G. Sirri, L. D. Spencer, R. Sunyaev, A. S. Suur-Uski, J. A. Tauber, D. Tavagnacco, M. Tenti, L. Toffolatti, M. Tomasi, T. Trombetti, L. Valenziano, J. Valiviita, B. Van Tent, L. Vibert, P. Vielva, F. Villa, N. Vittorio, B. D. Wandelt, I. K. Wehus, M. White, S. D. M. White, A. Zacchei, and A. Zonca, arXiv e-prints , arXiv:1807.06209 (2018), arXiv:1807.06209 [astro-ph.CO].

[20] Planck Collaboration, R. Adam, P. A. R. Ade, N. Aghanim, M. Arnaud, M. Ashdown, J. Aumont, C. Baccigalupi, A. J. Banday, R. B. Barreiro, and et al., Astron. Astrophys. **594**, A9 (2016), arXiv:1502.05956.

[21] Planck Collaboration, P. A. R. Ade, N. Aghanim, M. Arnaud, M. Ashdown, J. Aumont, C. Baccigalupi, A. J. Banday, R. B. Barreiro, J. G. Bartlett, and et al., Astron. Astrophys. **594**, A12 (2016), arXiv:1509.06348.

[22] A. Cooray, M. Kamionkowski, and R. R. Caldwell, Phys. Rev. D **71**, 123527 (2005), astro-ph/0503002.

SUPPLEMENTAL MATERIAL

In this supplementary material, we describe various trispectrum components for the patchy-reionization related estimators, including realization dependent biases, estimator-based biases and higher order (N_1) biases.

Appendix A: Trispectrum components for patchy-reionization related estimators

The weighting functions and normalization factors for estimators of gravitational lensing and anisotropic optical depth are given in Table I, where the F and J matrix are multipole-weighted 3-j Wigner symbols [4, 8]. Symbols $\tilde{C}_\ell$ and C_ℓ refer to unlensed and noise-included CMB power spectra.

A four-point correlation function is constructed from four CMB maps X, Z, W and V. $\{X, Z, W, V\} = \{T, E, B\}$. We make simulations for a map set for lensing potential ($\phi^{(\mathrm{un})}, \phi^{(\phi)}, \phi^{(\tau)}, \phi^{(\mathrm{f})}, \phi^{(\mathrm{G})}$). Here the superscripts "(un)", "(ϕ)", "(τ)", "(f)" and "(G)", refer to unlensed, ϕ-only, τ-only, $\phi+\tau$, and Gaussian simulations. The same map set is also made for τ reconstruction. In the following, operators $\{A, B\} = \{\phi, \tau\}$. Generally, the four-point correlation function is expressed as

$$C_\ell^{A \times B, cd} = \langle A(X^{(c)}, Z^{(c)}) B(W^{(d)}, V^{(d)}) \rangle, \tag{A1}$$

where the superscript "c" or "d" refers to a specific type of CMB map in the map set, and A or B refers to an estimator operator ϕ or τ.

The realization dependent (RD) bias is calculated from

$$N_{0,\ell}^{A \times B, cd}(XZ; WV) = \langle [A(X^{(D)}, Z^{(c)}) + A(X^{(c)}, Z^{(D)})][B(W^{(D)}, V^{(c)}) + B(W^{(c)}, V^{(D)})] \rangle$$
$$- \langle A(X^{(c)}, Z^{(c')})[B(W^{(d)}, V^{(d')}) + B(W^{(d')}, V^{(d)})] \rangle. \tag{A2}$$

Here the superscript "(D)" refers to the data. We make two map realizations labeled as (X, Z, W, V) and (X', Z', W', V').

The estimator for the anisotropic optical depth $\langle \tau \tau \rangle$ is defined as

$$\hat{C}_\ell^{\tau\tau} = \langle [\tau(X^{(f)}, Z^{(f)}) - \tau(X^{(\phi)}, Z^{(\phi)})][\tau(W^{(f)}, V^{(f)}) - \tau(W^{(\phi)}, V^{(\phi)})] \rangle. \tag{A3}$$

In the following, the average symbol $\langle \rangle$ and subscript ℓ are omitted for brevity. Eq. A3 can be decomposed into a few components. The raw signal is

$$\tilde{C}^{\tau\tau} = \tau(X^{(f)}, Z^{(f)}) \tau(W^{(f)}, V^{(f)}), \tag{A4}$$

and the raw lensing-induced trispectrum is

$$\tilde{C}^{\tau\tau,\phi} = \tau(X^{(f)}, Z^{(f)}) \tau(W^{(\phi)}, V^{(\phi)}) + \tau(X^{(\phi)}, Z^{(\phi)}) \tau(W^{(f)}, V^{(f)}) - \tau(X^{(\phi)}, Z^{(\phi)}) \tau(W^{(\phi)}, V^{(\phi)}), \tag{A5}$$

which is related to a pure lensing bias as $C^{\tau\tau,\phi} = \tilde{C}^{\tau\tau,\phi} - C^{\tau\tau,G}$, and $C^{\tau\tau,G}$ is the Gaussian bias.

The N1 bias for $\tau\tau$ ($A = \hat{\tau}$, $B = \hat{\tau}$, $c = d =$"(τ)") is

$$N_{1,\ell}^{A \times B, cd}(XZ; WV) = \langle A(X^{(c)}, Z^{(c')})[B(W^{(d)}, V^{(d')}) + B(W^{(d')}, V^{(d)})] \rangle$$
$$- \langle A(X^{(c)}, Z^{(c'')})[B(W^{(d)}, V^{(d'')}) + B(W^{(d'')}, V^{(d)})] \rangle,$$

where two realizations X, Z, W, V and X', Z', W', V' are created from the same ϕ or τ but different CMB and noise realizations.

With the components defined above, the reconstructed signal is expressed as

$$\hat{C}_\ell^{\tau\tau} = \tilde{C}_\ell^{\tau\tau} - C_\ell^{\tau\tau,\phi} - N_{0,\ell} - N_{1,\ell}, \tag{A6}$$

where the RD is subtracted instead of the Gaussian bias N_0 from simulations for the data.

The estimator of the cross-power spectrum $\langle \phi\tau \rangle$ is defined as

$$\hat{C}_\ell^{\phi\tau} = \langle [\phi(X^{(f)}, Z^{(f)}) - \phi(X^{(\tau)}, Z^{(\tau)})][\tau(W^{(f)}, V^{(f)}) - \tau(W^{(\phi)}, V^{(\phi)})] \rangle. \tag{A7}$$

The raw trispectrum is

$$\tilde{C}^{\phi\tau} = \phi(X^{(f)}, Z^{(f)}) \tau(W^{(f)}, V^{(f)}), \tag{A8}$$

TABLE I. The weighting functions for lensing (ϕ) and patchy reionization (τ) quadratic estimators [4, 8]

	$f^\phi_{\ell L \ell'}$	$f^\tau_{\ell L \ell'}$	$g^\phi_{\ell \ell'}(L)$	$g^\tau_{\ell \ell'}(L)$
TT	$\tilde{C}^{TT}_\ell {}_0F_{\ell' L \ell} + \tilde{C}^{TT}_{\ell'} {}_0F_{\ell L \ell'}$	$(\tilde{C}^{TT}_\ell + \tilde{C}^{TT}_{\ell'})J^{\ell L \ell'}_{000}$	$\dfrac{f^\phi_{\ell L \ell'}}{2 C^{TT}_\ell C^{TT}_{\ell'}}$	$\dfrac{f^\tau_{\ell L \ell'}}{2 C^{TT}_\ell C^{TT}_{\ell'}}$
EB	$\tilde{C}^{EE}_\ell {}_2F_{\ell' L \ell}$	$\tilde{C}^{EE}_\ell (J^{\ell' L \ell}_{-202} - J^{\ell L \ell'}_{20-2})/(2i)$	$\dfrac{f^\phi_{\ell L \ell'}}{C^{EE}_\ell C^{BB}_{\ell'}}$	$\dfrac{f^\tau_{\ell L \ell'}}{C^{EE}_\ell C^{BB}_{\ell'}}$

and the lensing-induced raw trispectrum is

$$\tilde{C}^{\phi\tau,\phi} = \phi(X^{(\tau)}, Z^{(\tau)})\tau(W^{(f)}, V^{(f)}) + \phi(X^{(f)}, Z^{(f)})\tau(W^{(\phi)}, V^{(\phi)}) - \phi(X^{(\tau)}, Z^{(\tau)})\tau(W^{(\phi)}, V^{(\phi)}),$$

(A9)

from which a pure lensing bias is defined as $C^{\phi\tau,\phi} = \tilde{C}^{\phi\tau,\phi} - C^{\phi\tau,G}$, and $C^{\phi\tau,G}$ is the Gaussian term estimated from Gaussian realizations.

The N1 bias for the cross-power spectrum is

$$N_{1,\ell} = N^{A\times B,(ff)}_{1,\ell} - N^{A\times B,(f\phi)}_{1,\ell} - [N^{A\times B,(\tau f)}_{1,\ell} - N^{A\times B,(\tau\phi)}_{1,\ell}],$$

(A10)

where $A = \hat{\phi}$, $B = \hat{\tau}$, and each term has a general form

$$N^{A\times B,cd}_{1,\ell}(XZ;WV) = \langle A(X^{(c)}, Z^{(c')})[B(W^{(d)}, V^{(d')}) + B(W^{(d')}, V^{(d)})]\rangle.$$

(A11)

With the components defined above, the reconstructed signal is expressed as

$$\hat{C}^{\phi\tau}_\ell = \tilde{C}^{\phi\tau}_\ell - C^{\phi\tau,\phi}_\ell - N_{0,\ell} - N_{1,\ell},$$

(A12)

where the RD is subtracted instead of the Gaussian bias N_0 from simulations for the data.